MASTER'S DEGREE THESIS

Master of Science in Advanced Mathematics and Mathematical Engineering

Title: Numerical model of cadiac electromechanics

Author: Nora Wieczorek i Masdeu

Advisor: Blas Echebarria and Pablo Sáez

Academic year: 2018-2019

UNIVERSITAT POLITÈCNICA DE CATALUNYA
BARCELONATECH
Facultat de Matemàtiques i Estadística

Universitat Politècnica de Catalunya

Facultat de Matemàtiques i Estadística

Master's degree thesis

Numerical model of cadiac electromechanics

Nora Wieczorek i Masdeu

ADVISORS:

Blas Echebarria and Pablo Sáez

October 1, 2019

Acknowledgements

I would like to thank my advisors, Blas Echebarria and Pablo Saéz, for their help and patience throughout the completion of the thesis.

Abstract

In this project, we develop a Finite Element Method (FEM) formulation that solves the cardiac electrophysiological problem of a three dimensional piece of tissue. This problem is modeled by an electromechanical model that includes the activation of a tension that depends on the cell's transmembrane potential and induces the contraction of the tissue. After applying an implicit time discretization, we end with a nonlinear system that depends on the position and potential at each node. This system is solved using the Newton-Raphson's method at each time iteration. Using this resolution methodology, we present a full implicit scheme. We also implement a faster and less accurate way of solving the coupled system with a staggered scheme: first computing the change of potential, and then actualizing the position of every node. Then, we simulate the electrophysiological model to observe the effect of the grid affects on the results. Finally, using the staggered algorithm, we simulate the propagation of a plane wave and the subsequent tissue contraction.

Contents

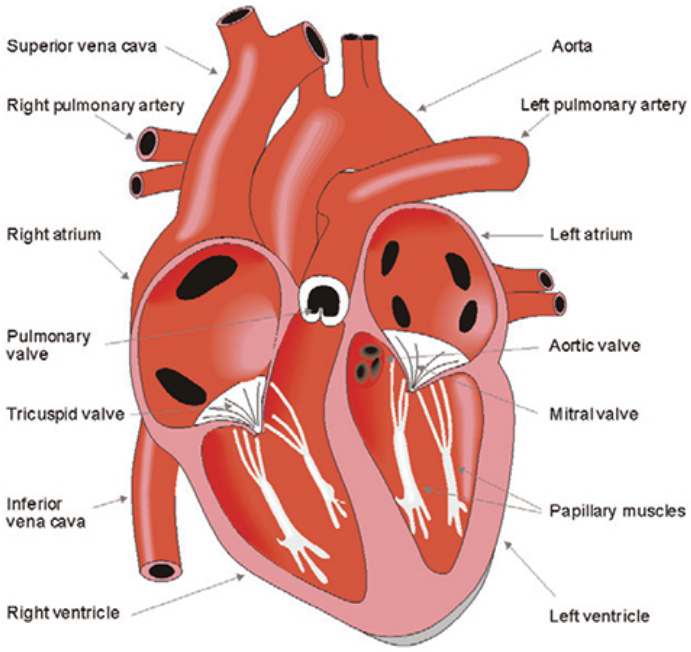

Figure 1: Structure of the heart. From [1].

1 Introduction

Nowadays, about a third of the world's deaths are associated to cardiovascular diseases. These diseases can be related to problems in the veins and arteries, which produce heart attacks and strokes, or to problems in the heart's contraction and, consequently, with the correct expulsion and distribution of the blood to our body.

The heart's contraction is produced by a change in the membrane potential of the myocytes, the muscular cardiac cells. An electrical pulse is originated on the sinusoidal node, our natural peacemaker. Then the wave is propagated along the tissue using the cardiac fibers that are composed by myocytes. This electrical wave is a result of the movement of different ions along the cells. The change of ions concentrations induces a contraction of the fibers, and consequently, to the whole heart's contraction, first on the atria and then on the ventricles, structure that we can see in Fig. 1.

These phenomena can be studied based on experimental data. For the mechanics, the ultrasounds permit the observation of the change of positions for every layer of muscle, whereas for the electrophysiology, optical mapping is applied and only permits to observe

the potential on the surface of the heart. To study the coupling phenomena, we can also simulate the hearts movement applying numerical methods to electromechanical models. This implementation gives us the advantage that both, the electrophysiology and the mechanics, are given at each point of the tissue. This simulations also permit us to check if the models that describe the coupling are well assumed, an consequently, a better understanding on how is this electromechanical coupling.

To obtain the simulations, we will need an electrical model for the wave propagation, a mechanical model for the stretch of the fibers, an finally, a coupling of the two models that can simulate how the change of potential induces a movement and/or how the stretch of the cells affects on some ionic channels. There are many proposals to model these situations such as the ones we can find on [3] and [4].

1.1 Physiology of a cardiac myocyte

Since the principal function of the heart is to pump the blood, the majority of its cells are muscular cells, called myocytes. They have a length of $80 - 100\mu m$ and a diameter of $10 - 20\mu m$. As we said, these cells respond with a mechanical movement to the electrical pulse.

1.1.1 Electro physiology

The myocytes have a selective permeability membrane that permits the circulation of Na^+, Ca^{2+}, K^+ and Cl^- ions through the ionic channels that open or close depending on the potential difference between the inside and outside of the cell at each instant.

When it is at resting state, the membrane potential is about $-85mV$. Upon electrical stimulation, this potential increases above a potential threshold and the cell produces a response called action potential. The amplitude of this answer is of $130mV$ approximately as can be observed in Fig. 2. Systems with this behaviour are called excitable and present two main characteristics. They have an attractor fixed point where all the orbits always return, after an small path if the stimulus strength was under a threshold, or after a larger one otherwise. In our case, this fixed point is the resting state. The second characteristic is

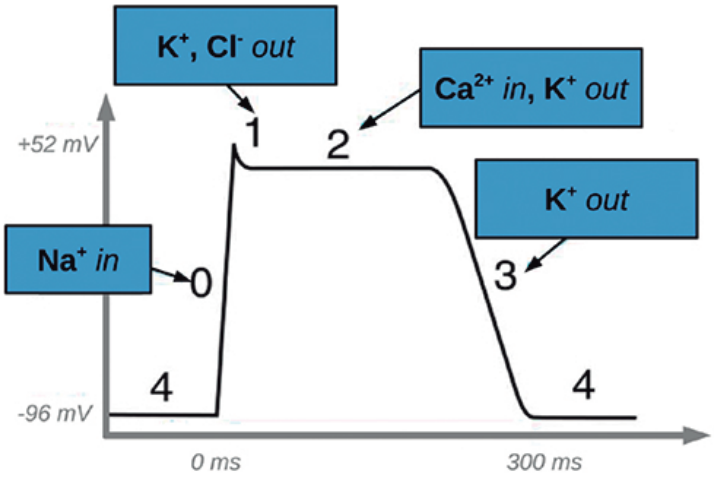

Figure 2: Action potential of a myocyte. From [2].

that after a big orbit, the system needs to stay in the fixed point for a while before an other high stimulus. This can be translated in the heart's system by: after an electrical wave and consequently, a contraction, the tissue needs to be at resting state before producing the next action potential.

The action potential has a particular form depending on the ion flux in the cell. Firstly, at phase 0, we see very fast entrance of the sodium ions (Na^+). Secondly, at phase 1, the cell ejects the potassium and chlorine ions (K^+ and Cl^-). To equilibrate it, at phase 2, calcium ions (Ca^{+2}) enter into the cell that produces the cell contraction. Once the calcium injection has finished, at phase 3, potassium ions emerge producing a decreased on the potential, that returns to the diastole or resting state at phase 4.

1.1.2 Mechanical response

As we previously said, the entrance of calcium ions generates the contraction. This entrance produces an openning of the Ryanodine Receptors that are located at the sarcoplasmic reticulum, where the concentration of calcium is 1000 times larges than in the cytosol. This process is known as calcium induced release. When the concentration at the cytosol increases the calcium ions stack to a protein called troponim C, changing its form and generating the contraction on the muscular fiber. In Fig. 3, we can observe how these variables: potential, calcium concentration and contraction, are related. Due to

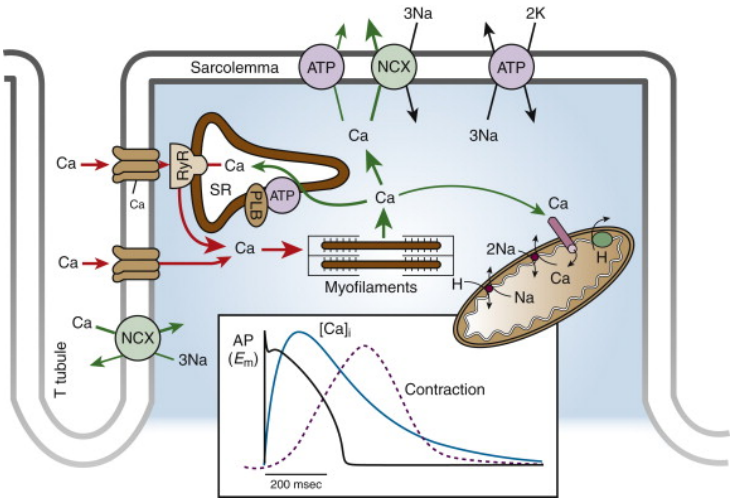

Figure 3: Potential, calcium concentration and contraction relation. From [14]

the fact of this fiber-direction dependency and the combination of contractile and passive material, the cardiac tissue presents a high anisotropy on the contraction.

1.2 Objectives

The main objective of this thesis is to develop a code that simulates a three dimensional piece of cardiac tissue from the electrical and mechanical perspectives.

To do so, we will consider 2 coupled simplified models: one for the electrophysiology of the myocytes and an additive formulation of the passive, induced by the tissue movement, and active deformation, produced by the change of potential at each point of the tissue, and we will apply the Finite Element Method to simulate them for a period of time.

First, we will solve it just for the electrical case, and then we will add to the resolution the mechanical terms.

Finally, we will compare the obtained results changing the parameters that will descrive our models.

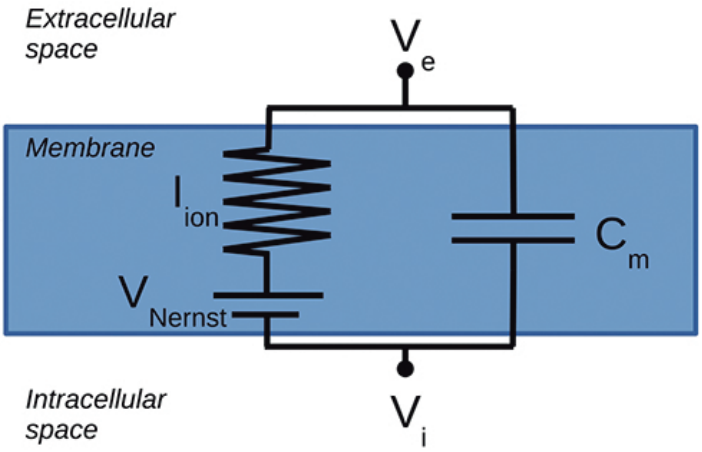

Figure 4: Electric scheme of the myocyte membrane. From the article [2]

2 Constitutive model of electromechanics

In this section, we will describe the models considered for the electromechanical behaviour of the myocardial tissue.

2.1 Electrophysiological model

As we said in section 1.1.1, the myocytes membrane has a selective permeability that permits the transport of ions through channels. This implies a difference between ions concentrations and, consequently, in a difference of potentials between the inside and the outside of each cell.

To model this behaviour, we can assimilate the cells membrane to a capacitor that stores electrical charge. For this reason, we can suppose that our cell follows the electrical scheme that presented in Fig. 4.

The two currents that we have to take into account are the one produced by the ions concentrations I_{ion} and the other one that represents the stored charge on the membrane. Since total charge is conserved, $I_{ion} + I_c = 0$.

On the other hand, we know that the stored charge is $Q = C_m V_m$ where C_m is the capacitance and V_m is the potential's difference. We also have that the current is the

charge per unit of time and the capacitance is constant along the time. Thus we end with

$$I_c = \frac{dQ}{dt} = C_m \frac{dV_m}{dt} \tag{1}$$

Substituting in the charge conservation equation:

$$C_m \frac{dV_m}{dt} + I_{ion} = 0 \tag{2}$$

where $V_m = V_i - V_e$ is the membrane voltage, i.e. the difference between the interior and exterior potentials.

For each type of ion X, we will model their currents using the expression $I_X = g_X(V_m - V_{Nernst,X})$, where $V_{Nerst,X}$ is the Nerst potential and $g_X = 1/r_X$ is the membrane conductance for the X ion. The Nerst potential can be written as:

$$V_{Nernst,X} = V_{i,X} - V_{e,X} = \frac{k_B T}{q} ln(c_{e,X}/c_{i,X}) \tag{3}$$

where $V_{i,X}$ and $V_{e,X}$ are the resulting interior and exterior potentials for the X ion, $c_{i,X}$ i $c_{e,X}$ are the interior and exterior concentrations, k_B is the Bolzmann's constant, T the temperature and $q = z|e|$ is the charge for one ion (z is the Valence and $|e|$ is the electron electrical charge).

The first model that considered this expressions for the ionic currents, was the Hodgkin-Huxley model on the 1952, that was applied to neurons. Thus, the total ionic charge is:

$$I_{ion} = \sum_X g_X(V_m - V_X) \tag{4}$$

After that, following the same formulation, more models where developed as the Noble model [5] on the 1962 and the Beeler-Reuter model [6] on the 1977. Nowadays, there exist a lot of models that include all kinds of cells that we can find on the humans heart. We can see some examples in [7].

On this report we will consider a simpler model, presented in [8], that will only include potassium and sodium ions. This will give us a similar to small animals hearts signal. Since there is no calcium phase 2 (Fig. 2) does not exist, what implies an action potential with a triangular form as we can see in Fig. 5.

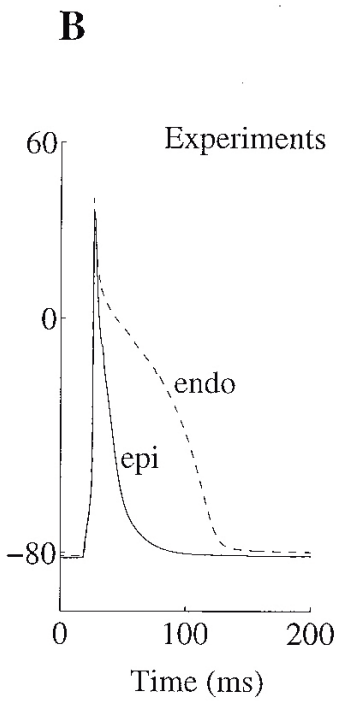

Figure 5: Action potential of a rat. From [9]

We will consider the following action potential:

$$\frac{dV}{dt} = -\frac{I_{Na} + I_K + I_{stim}}{C_m} \tag{5}$$

where I_{stim} is the stimulus originated in the sinusoidal node.

To simulate the ionic gates opening, we will use a smoothed Heaviside function $S_\epsilon(V)$ as we can see in Fig. 6,

$$S_\epsilon(V) = \frac{1 + \tanh\left(\frac{V - V_c}{\epsilon}\right)}{2} \xrightarrow[\epsilon \to 0]{} S(V) = \begin{cases} 1 & V > V_C \\ 0 & V < V_C \end{cases} \tag{6}$$

The potassium ionic current will be modeled by the Eq. (7), that is an increasing line when the potential is under a threshold (V_C) and is a constant function when otherwise. The sodium, I_{Na}, behaves in the other way, and depends on the probability of the gate for being open, $h(V)$ that follows its own coupled ode as we can see in Eq. (8) and Eq.

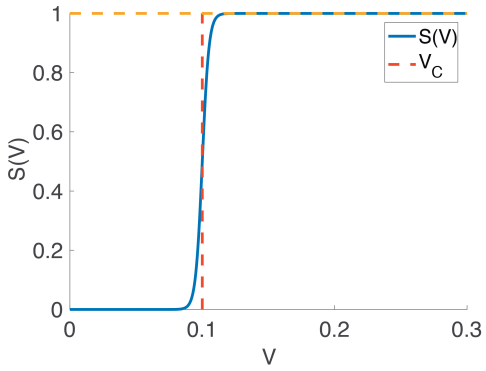

Figure 6: Smoothed Heaviside function $S(V)$.

(9). We can see this currents represented for $h = 1$ at Fig.7.

$$\widetilde{I_{K\epsilon}} = \frac{I_{K\epsilon}}{C_m} = \frac{1}{\tau_0}\left[S(V) + (1 - S(V))\frac{V}{V_C}\right] \xrightarrow[\epsilon\to 0]{} \widetilde{I_K}(V) = \begin{cases} \frac{1}{\tau_0} & V > V_C \\ \frac{1}{\tau_0}\frac{V}{V_C} & V < V_C \end{cases} \tag{7}$$

$$\widetilde{I_{Na\epsilon}} = \frac{I_{Na\epsilon}}{C_m} = -\frac{S(V)h}{\tau_A} \xrightarrow[\epsilon\to 0]{} \widetilde{I_{Na}}(V) = \begin{cases} -h/\tau_A & V > V_C \\ 0 & V < V_C \end{cases} \tag{8}$$

$$\frac{dh}{dt}_{\epsilon} = \frac{1 - S(V) - h}{\tau_-(1 - S(V)) + \tau_+ S(V)} \xrightarrow[\epsilon\to 0]{} \frac{dh}{dt}(V) = \begin{cases} -h/\tau_+ & V > V_C \\ (1-h)/\tau_- & V < V_C \end{cases} \tag{9}$$

To induce a longer response of the system we will introduce an stimulation current I_{stim} to simulate the current that generates the sinusoidal node, that will only depend on the time, and it will be T-periodic as we can see in Fig. 7).

$$\widetilde{I_{stim}}(t) = \frac{I_{stim}}{C_m}(t) = \begin{cases} H & \text{t (mod T)} < tt \\ 0 & \text{otherwise} \end{cases} \tag{10}$$

where H is the intensity of the stimulus, tt the amplitude and T the period.

As in many other situations in biology [10], the cardiac cells behave as an excitable system. They have a fixed point, the resting situation, and when we apply small perturbation, an small pulse, they return very fast to the fixed point. On the other hand, when a more intense pulse that makes it increase above a threshold, V_C, the system responds with a more extensive orbit, and needs to stay into fixed point for a while to return to repeat it. This property can be seen in Fig. 8.

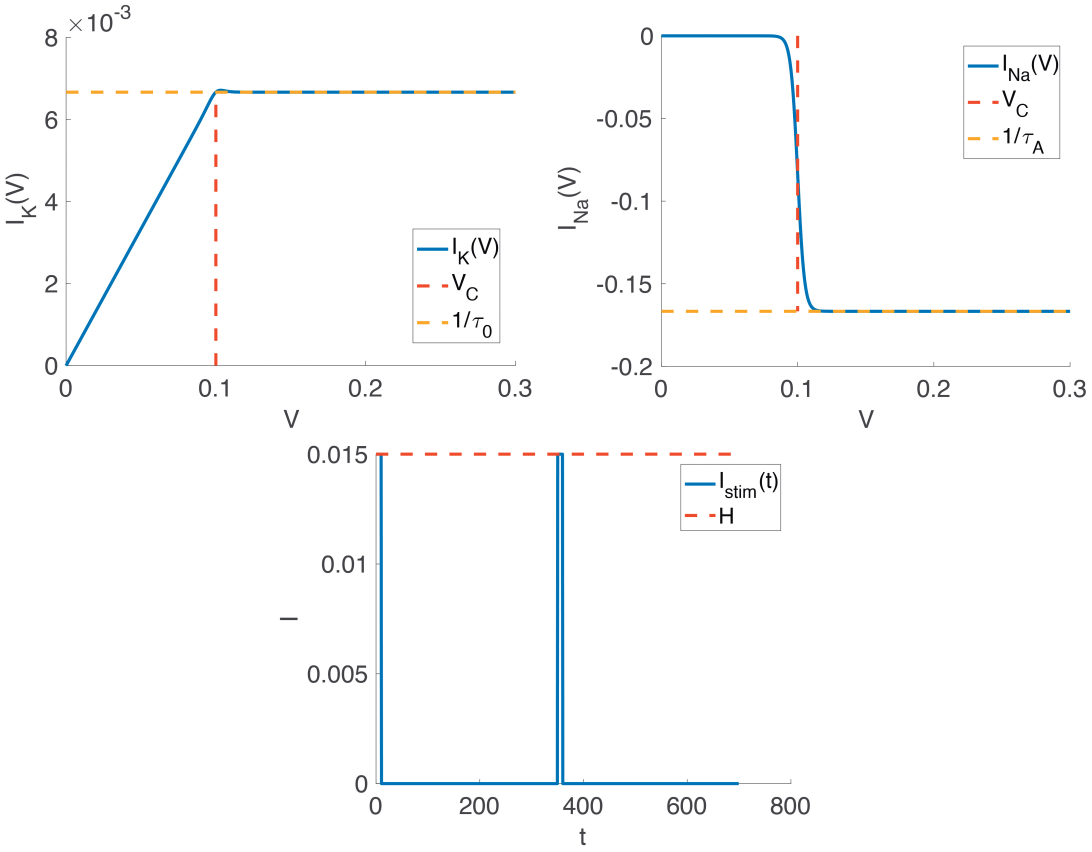

Figure 7: Graphical representations of I_{Na}, I_K and I_{stim} for $h = 1$

Then, each cell electric comportment will we model by the following system of equations.

$$\frac{dV}{dt} = g_V(V,h,t) = -\frac{S(V) + [1 - S(V)]V/V_c}{\tau_0} + \frac{S(V)h}{\tau_A} + I_{stim}(t) \tag{11}$$

$$\frac{dh}{dt} = g_h(V,h,t) = \frac{1 - S(V) - h}{\tau_-[1 - S(V)] + S\tau_+} \tag{12}$$

In Fig. 9, we can see its representation for T = 400 ms. Since the tissue will we formed by cardiac cells, we will have to add a term that models its coupling between cells. The different ions flow from one cell to the other through the gap junctions. This phenomenon gives rise to diffusion on the membrane's potential, which can be mathematically described as:

$$\frac{\partial V}{\partial t} = \nabla \cdot (D\nabla V) - g_V(V,h,\mathbf{x},t) \tag{13}$$

where D is the diffusion that depends on the direction of the fibers.

Since the pulse is only applied to part of the domain and then propagated, I_{stim} will also depend on the position. In our case we will impose that the pulse is given on the $\{X = 0\}$

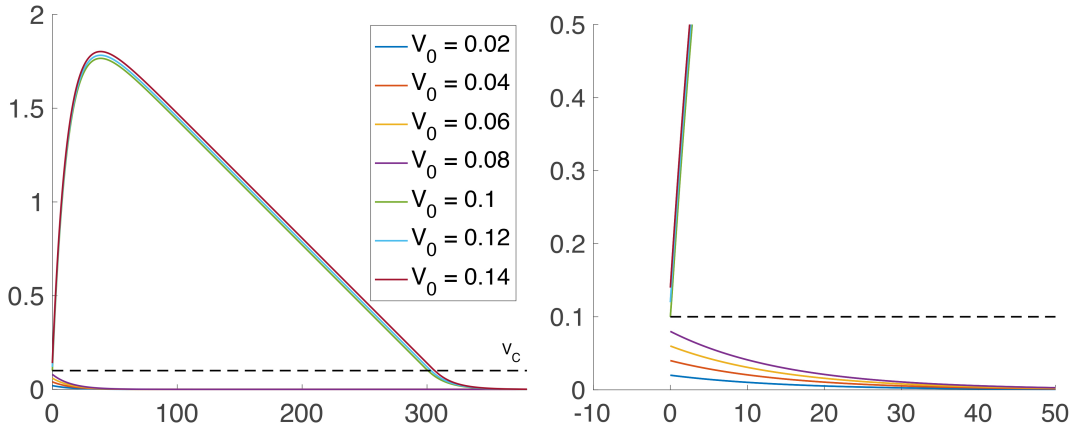

Figure 8: Numerical test of the excitability of the system, obtained results with initial conditions V_0 with values between 0.2 and 1.4 and $h_0 = 1$.

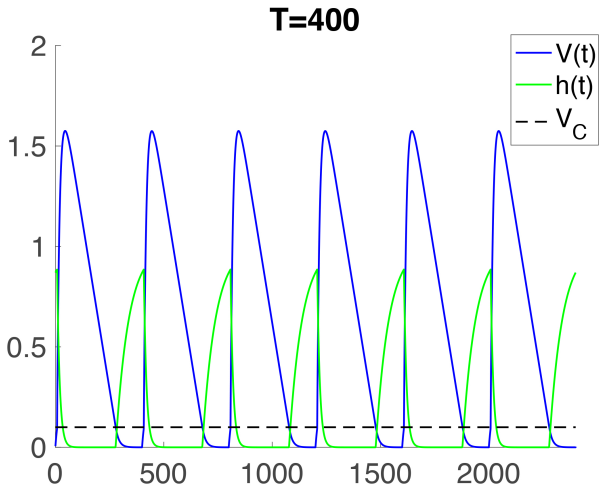

Figure 9: Electrical model for T = 400 ms.

side of the tissue.

Finally, since we consider that there no flux of electrical current (ions) to the surrounding medium we will impose natural Neumann conditions on the whole boundary , i.e. $D\nabla V(\mathbf{x}, t)) = 0 \ \forall (\mathbf{x}, t) \in \delta\Omega \times (0, t_{end}]$.

2.2 Mechanical model

As has been described in [13], the spatial motion of a body that has initial positions $\mathbf{X}$ (material coordinates), can be described using the spatial motion map as $\mathbf{x} = \boldsymbol{\varphi}(\mathbf{X}, t)$:

$\Omega_0 \times \mathbb{R} \rightarrow \Omega_t$, where Ω_0 is the initial domain and Ω_t is the deformed domain a time t.

Then, the deformation gradient $\mathbf{F}$ is defined as the spatial derivative of the deformation map with respect to the initial configuration $\mathbf{X}$, that is, $\mathbf{F} = \nabla_{\mathbf{X}}\varphi$ where the jacobian is $J = det(\mathbf{F})$.

Another important variable in the mechanic study is the Cauchy-Green deformation tensor $\mathbf{C}$, that defines relevant strain measures and is computed as $\mathbf{C} = \mathbf{F^t}{\cdot}\mathbf{F}$. Finally, $I_1 = tr(\mathbf{C})$ is the first strain invariant.

As we previously said, the myocardial tissue is an hyperelastic material. This property can be mathematically described using the Clausius-Planck form of the second law of thermodynamics, that reads

$$\mathcal{D}_{int} = \frac{1}{2}\mathbf{S} : \dot{\mathbf{C}} - \dot{\mathbf{\Psi}} - S_0\theta = [\mathbf{S} - 2\partial_{\mathbf{C}}\mathbf{\Psi}] : \dot{\mathbf{C}} - S_0\theta \geq 0, \tag{14}$$

where $\mathcal{D}_{int}$ is the dissipation of the internal energy, $\mathbf{S}$ is the second Piola-Kirchoff stress tensor, $\mathbf{\Psi}$ is the strain energy density function (SEDF), S_0 is the material form of the internal dissipation and θ is the entropy. In our case, we will make two assumptions: the thermal effects will be negligible, so S_0 and θ will be omitted; and the material will be assumed as perfectly elastic, leading to the degeneration of the inequality of Eq. (14) into

$$(\mathbf{S} - 2\partial_{\mathbf{C}}\Psi) : \dot{\mathbf{C}} = 0 \tag{15}$$

As $\mathbf{C}$, and consequently $\dot{\mathbf{C}}$ can be different to zero, the first term should be null, thus, in this case the second Piola-Kirchoff stress tensor is

$$\mathbf{S} = 2\frac{\partial\Psi}{\partial\mathbf{C}} \tag{16}$$

Given this tensor, the first Piola-Kirchoff can be obtained by pulling it back to the reference configuration, i.e. $\mathbf{P} = \mathbf{F} \cdot \mathbf{S}$. Using Eq. 16, the first Piola-Kirchoff stress tensor can be also described as a function of SEDF, resulting of the following expression

$$\mathbf{P} = \frac{\partial\Psi}{\partial\mathbf{F}} \tag{17}$$

We will consider a classical Neo-Hookean SEDF model to define the energy, $\Psi(\mathbf{C}) = \Psi_{vol}(J) + \Psi_{ich}(\mathbf{C})$. Therefore, the energy function reads

$$\mathbf{\Psi}(\mathbf{C}) = \frac{1}{2}\lambda\ln^2(J) - \frac{1}{2}\mu\ln(J) + \frac{1}{2}\mu[I_1 - 3] \tag{18}$$

where λ and μ are the Lamme parameters which describe the mechanical properties of a material. By deriving this expression by C, we obtain the second Piola-Kirchoff stress tensor $\mathbf{S}$, and consequently, the first Piola-Kirchoff stress tensor $\mathbf{P}$

$$\mathbf{S} = [\lambda \ln(J) - \mu]\mathbf{C}^{-1} + \mu\mathbf{I} \Rightarrow \mathbf{P} = [\lambda \ln(J) - \mu]\mathbf{F}^{-1} + \mu\mathbf{F} \tag{19}$$

2.3 Coupling electromechanics

In the previous section we were discussing the mechanical response that the body has to a deformation, that is called passive reaction. To induce a mechanical contraction from the change of potential, we will include and additive active stress to the first Piola-Kirchoff stress tensor, $\mathbf{P} = \mathbf{P^{pas}} + \mathbf{P^{act}}$, where $\mathbf{P^{pas}}$ is equal to $\mathbf{P}$ from Eq. (19). To generate this active reaction, we base our model on the propose of Nach and Panfilov [4], as we can see in [11] and [12]. We assume that an increase on the membrane potential induces a contraction F^{act} that acts along the fiber direction $\mathbf{f_0}$. This contractile force F^{act} presents a twitch-type behaviour with an smooth transition as we can see in Fig. 10. To have this behaviour, we modeled using a Heaviside function $\epsilon(V)$ that is ϵ_0 for V under a threshold ($\bar{V}$) and ϵ_∞ otherwise.

$$\begin{aligned}
\mathbf{P^{act}} &= F^{act}(V)\mathbf{f_0} \otimes \mathbf{f_0} && (20)\\
\frac{dF^{act}}{dt} &= \epsilon(V)[k_F(V - V_r) - F^{act}] && (21)\\
\epsilon(V) &= \epsilon_0 + (\epsilon_\infty - \epsilon_0)e^{-e^{-\xi(V-\bar{V})}} && (22)
\end{aligned}$$

where k_F controls the saturation of F^{act}, V_r is the resting potential and $\bar{V}$ is the limit value above which contraction is initiated.

Finally, we can model the tissue mechanics of the coupled model using the balance equation obtained from the principle of virtual work in continuum mechanics, that balances the rate of change of the linear momentum with the divergence of the momentum flux,

$$\nabla \cdot \mathbf{P} + \mathbf{F}^{\varphi} = \mathbf{0} \quad in\, \Omega \tag{23}$$

where $\mathbf{F}^{\varphi}$ is the momentum source and is equal to zero since it characterizes volume forces such as gravity, that we assume to be negligibly small.

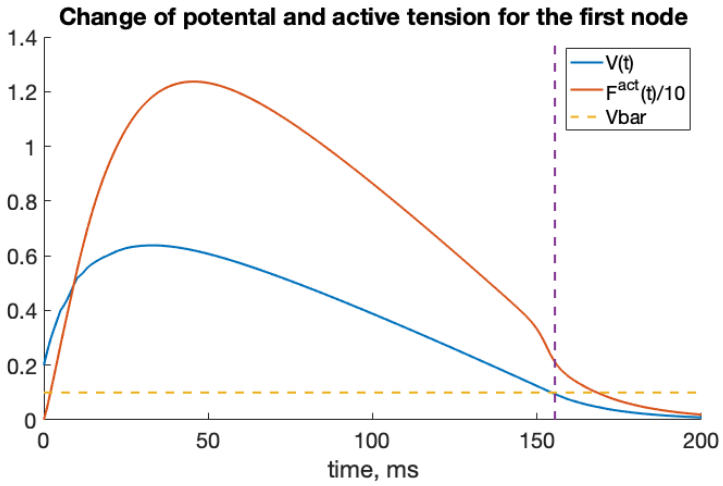

Figure 10: Graphical representation of the active force for the central node and a stretch for $k_F = 15$

3 Numerical implementation

In this section, we will describe the discretized formulation in space, with finite element method, and in time, with an implicit Euler, used to implement the simulation of the coupled electromechanical model on the three dimensional tissue with initial configuration Ω_0.

3.1 Full implicit coupled resolution of the problem

We define as the **strong form** of our problem the following mechanical and electrophysiological balance equations in they residual form, where we had not considered the strech-induced change in the propagation speed, what makes D constant,

$$\mathbf{R}^{\varphi}(V,\varphi) = \nabla \cdot (\mathbf{P}^{\mathbf{act}}(F^{act}(V)) + \mathbf{P}^{\mathbf{pas}}(\varphi)) = \mathbf{0} \tag{24}$$

$$R^{V}(V,h,\mathbf{X},t) = \frac{\partial V}{\partial t} - \nabla \cdot (D \cdot \nabla V) - g_V(V,h,\mathbf{X},t) = 0 \tag{25}$$

in $\Omega(t) \times (0, t_{end}]$. Where $\dot{F^{act}} = g_F(F^{act}, V)$ and $\dot{h} = g_h(V, h)$ and with the following Dirichlet and Neumann boundary conditions,

$$\begin{aligned} \varphi &= \bar{\varphi} \quad on\, \Gamma_D^{\varphi} \\ V &= \bar{V} \quad on\, \Gamma_D^{V} \\ \mathbf{P} \cdot \mathbf{n} &= \bar{\mathbf{T}}^{\varphi} \quad on\, \Gamma_V^{\varphi} \\ (\mathbf{D} \cdot \nabla V) \cdot n &= \bar{\mathbf{T}}^{\mathbf{V}} \quad on\, \Gamma_N^{V} \end{aligned}$$

where $\bar{\varphi}$ and $\bar{V}$ are prescribed values for the unknowns, $\mathbf{n}$ is the outward normal unitary vector to the boundary Γ and $\bar{\mathbf{T}}^{\varphi}$ and $\bar{\mathbf{T}}^{\mathbf{V}}$ are the prescribed fluxes on the boundary.

Recalling the Hilbert spaces we define:

$$\begin{aligned} \mathcal{S}^{\varphi} &= \{\varphi \in \mathcal{H}^1(\Omega) | \varphi = \bar{\varphi}\, on\, \Gamma_D^{\varphi}\} \\ \mathcal{S}^{V} &= \{V \in \mathcal{H}^1(\Omega) | V = \bar{V}\, on\, \Gamma_D^{V}\} \\ \mathcal{V}^{\varphi} &= \{\tilde{\varphi} \in \mathcal{H}^1(\Omega) | \tilde{\varphi} = 0\, on\, \Gamma_D^{\varphi}\} \\ \mathcal{S}^{V} &= \{\tilde{V} \in \mathcal{H}^1(\Omega) | \tilde{V} = 0\, on\, \Gamma_D^{\varphi}\} \end{aligned}$$

3.1.1 Weak form of the problem

In order to find the weak form of the problem, we consider two functions: $\tilde{\varphi} \in \mathcal{V}^{\varphi}$ and $\tilde{V} \in \mathcal{V}^{V}$, and we integrate its product with $\mathbf{R}^{\varphi}$ and R_V along the spatial domain Ω, that will be Ω_{t*} at the time instant $t*$. Applying the divergence theorem and imposing the boundary conditions to $\delta\Omega = \Gamma_D^{\varphi} \cup \Gamma_N^{\varphi} = \Gamma_D^{V} \cup \Gamma_N^{V}$ we end with the **weak form** of the problem.

$$\begin{aligned} \int_{\Omega} \nabla\tilde{\varphi}(\mathbf{x}) : \mathbf{P}\, d\Omega - \int_{\Gamma_N^{\varphi}} \tilde{\varphi}(\mathbf{x}) \bar{\mathbf{T}}^{\varphi}\, d\Omega &= 0 \\ \int_{\Omega} \tilde{V} \frac{\partial V}{\partial t}\, d\Omega + \int_{\Omega} \nabla\tilde{V} \cdot (D \cdot \nabla V)\, d\Omega - \int_{\Omega} \tilde{V} g_V(V, h, \mathbf{x}, t)\, d\Omega - \int_{\Gamma_N^{V}} \tilde{V}(\mathbf{x}) \bar{\mathbf{T}}^{\mathbf{V}}\, d\Omega &= 0 \end{aligned}$$

As $\bar{\mathbf{T}}^{\varphi} = 0$ and $\bar{\mathbf{T}}^{\mathbf{V}} = 0$, from now on we will delete this terms.

3.1.2 Space discretization

Considering a finite elements space discretization $\Omega = \cup_{e=1}^{n_{Elem}} \Omega_e$ with nodes $\{\mathbf{x_i}\}_{i=1}^{n_{Nodes}}$ we define a linear basis $\{N_i(\mathbf{x})\}_{i=1}^{n_{Nodes}}$ such that $N_i(\mathbf{x_j}) = \delta_{ij}$.

To find the finite elements solution we will approximate the position map and potential scalar function at each time instant t^* as

$$\begin{aligned} \boldsymbol{\varphi}(\mathbf{X}, t^*) &\approx \boldsymbol{\varphi}^h(\mathbf{x}, t^*) = \sum_{j=1}^{n_{Nodes}} (\varphi_j^x(t^*), \varphi_j^y(t^*), \varphi_j^z(t^*))^T N_j(\mathbf{x}) \\ V(\mathbf{x}, t) &\approx V^h(\mathbf{x}, t) = \sum_{j=1}^{n_{Nodes}} V_j(t) N_j(\mathbf{x}) \end{aligned}$$

To consider these approximations, we substitute in the terms of weak form , and also write $\tilde{\boldsymbol{\varphi}}$ and $\tilde{V}$ with the same basis notation. As the weak form has to we accomplished $\forall \tilde{\boldsymbol{\varphi}} \in \mathcal{V}^{\varphi}$ and $\forall \tilde{V} \in \mathcal{V}^{V}$, it has to we accomplished $\forall \tilde{\mathbf{V}} = (\tilde{V}_1, ...\tilde{V}_{n_{Nodes}}) \in \mathbb{R}^{n_{Nodes}}$ and $\forall \tilde{\boldsymbol{\varphi}} = (\tilde{\varphi}_1^x, \tilde{\varphi}_1^y, \tilde{\varphi}_1^z, ...\tilde{\varphi}_{n_{Nodes}}^z) \in \mathbb{R}^{3 \times n_{Nodes}}$. So, finding (φ, V) in the weak form will be equivalent to find them such that

$$\begin{aligned} &\int_{\Omega} \nabla N_i : (\mathbf{P^{act}}(F^{act}(V^h)) + \mathbf{P^{pas}}(\varphi^h))\, d\Omega = \mathbf{0} \\ &\sum_{j=1}^{n_{Nodes}} \dot{V}_j \int_{\Omega} N_i N_j \, d\Omega + \sum_{j=1}^{n_{Nodes}} V_j \int_{\Omega} \nabla N_i \cdot (D \cdot \nabla N_j)\, d\Omega - \int_{\Omega} N_i g_V(V^h, h^h, t)\, d\Omega = \mathbf{0} \end{aligned}$$

$\forall i = 1, ..., n_{Nodes}$.

3.1.3 Time discretization

In this section we will discuss the resolution of the following system of ODEs

$$\begin{aligned} \mathbf{R}^{\varphi} &= \mathbf{G}^{\varphi}(\boldsymbol{\varphi}(t), \mathbf{V}(t), \mathbf{F^{act}}(t)) = \mathbf{0} \\ \mathbf{R}^{\mathbf{V}} &= \mathbf{M}\dot{\mathbf{V}}(t) + \mathbf{K}\mathbf{V}(t) - \mathbf{G}^{\mathbf{V}}(\mathbf{V}(t), \mathbf{h}(t)) = \mathbf{0} \end{aligned}$$

where the matricial and vectorial components are

$$\begin{aligned}
\mathbf{G}^{\varphi}{}_{I} &= \int_{\Omega} \nabla N_i : (\mathbf{P^{act}}(F^{act}(V^h(t))) + \mathbf{P^{pas}}(\varphi^h(t)))\, d\Omega\, d\Omega \\
\mathbf{M}_{KL} &= \int_{\Omega} N_k N_l\, d\Omega \\
\mathbf{K}_{KL} &= \int_{\Omega} \nabla N_k \cdot (D \cdot \nabla N_l)\, d\Omega \\
\mathbf{G^V}{}_{K} &= \int_{\Omega} N_k g_V(V^h, h^h) d\Omega + \int_{\Omega} N_k \frac{I_{stim}}{C}\, d\Omega
\end{aligned}$$

Now, we will uniformly discretize the time considering the notation $t^n = n\Delta t$, using the Euler's implicit scheme. Then, at each time iteration, we will compute $(\boldsymbol{\varphi}^{n+1}, \mathbf{V}^n)$ as the solution of

$$\mathbf{R}^{\varphi,\mathbf{n}} = \mathbf{G}^{\varphi}(\boldsymbol{\varphi}^{n+1}, \mathbf{V}^{n+1}, \mathbf{F^{act}}^{n+1}) = \mathbf{0} \tag{26}$$

$$\mathbf{R}^{\mathbf{V},\mathbf{n}} = \frac{\mathbf{M}}{\Delta t}(\mathbf{V}^{n+1} - \mathbf{V}^n) + \mathbf{K^{VV}}\mathbf{V}^{n+1} - \mathbf{G^V}(\mathbf{V}^{n+1}, \mathbf{h}^{n+1}) = \mathbf{0} \tag{27}$$

3.1.4 Procedure to solve the discretized system

Since it is a system of non-linear functions, at each time iteration will use the Newton-Raphson's method to find the zero of Eq. (26) and Eq. (27).

As we have seen in the previous sections, these functions also depend on two time dependent variables, that are described by their own ODEs. To compute them at each time step we also use the Euler's implicit scheme and we find the analytical solutions $F^{act,n+1}$ and h^{n+1} as we can see in the following development.

$$\begin{aligned}
& \frac{F^{act,n+1} - F^{act,n}}{\Delta t} = \epsilon(V^{n+1})[k_F(V^{n+1} - V_r) - F^{act,n+1}] \\
\Rightarrow\ & F^{act,n+1} = \frac{F^{act,n} + \Delta t \epsilon(V^{n+1}) k_F(V^{n+1} - V_r)}{1 + \Delta t \epsilon(V^{n+1})} \qquad (28) \\
& \frac{h^{n+1} - h^n}{\Delta t} = \frac{1 - S(V^{n+1}) - h^{n+1}}{\tau_-(1 - S(V^{n+1})) + \tau_+ S(V^{n+1})} \\
\Rightarrow\ & h^{n+1} = \frac{(\tau_-(1 - S(V^{n+1})) + \tau_+ S(V^{n+1}))h^n + 1 - S(V^{n+1})}{\tau_-(1 - S(V^{n+1})) + \tau_+ S(V^{n+1}) + \Delta t} \qquad (29)
\end{aligned}$$

To sum up, we will apply the following scheme to find an approximate solution at each time iteration:

1. Given $(\boldsymbol{\varphi}^{\boldsymbol{n}}, \mathbf{V}^{\mathbf{n}}, \mathbf{F}^{\mathbf{act,n}}, \mathbf{h}^{\mathbf{n}})$ from the previous time step, we define $({}^{\mathbf{0}}\boldsymbol{\varphi}^{\boldsymbol{n+1}}, {}^{\mathbf{0}}\mathbf{V}^{\mathbf{n+1}}) = (\boldsymbol{\varphi}^{\boldsymbol{n}}, \mathbf{V}^{\mathbf{n}})$,

2. While $||(\mathbf{R}^{\boldsymbol{\varphi},\mathbf{n}}({}^{\boldsymbol{k}}\boldsymbol{\varphi}^{\boldsymbol{n+1}}, {}^{\mathbf{k}}\mathbf{V}^{\mathbf{n+1}}, {}^{\mathbf{k}}\mathbf{F}^{\mathbf{act,n+1}}), \mathbf{R}^{\mathbf{V},\mathbf{n}}({}^{\mathbf{k}}\mathbf{V}^{\mathbf{n+1}}, {}^{\mathbf{k}}\mathbf{h}^{\mathbf{n+1}}))|| > tol$,

   (a) We compute $({}^{\mathbf{k+1}}\mathbf{F}^{\mathbf{act,n+1k+1}}\mathbf{h}^{\mathbf{n+1}})$ using Eq. 28 and Eq. 29,

   (b) We update the variables $({}^{\boldsymbol{k+1}}\boldsymbol{\varphi}^{\boldsymbol{n+1}}, {}^{\mathbf{k+1}}\mathbf{V}^{\mathbf{n+1}})$ applying the Newton-Raphson's method,

$$\begin{bmatrix} {}^{\boldsymbol{k+1}}\boldsymbol{\varphi}^{\boldsymbol{n+1}} \\ {}^{\mathbf{k+1}}\mathbf{V}^{\mathbf{n+1}} \end{bmatrix} = \begin{bmatrix} {}^{\boldsymbol{k}}\boldsymbol{\varphi}^{\boldsymbol{n+1}} \\ {}^{\mathbf{k}}\mathbf{V}^{\mathbf{n+1}} \end{bmatrix} - \left(\frac{\boldsymbol{\partial}(\boldsymbol{R}^{\boldsymbol{\varphi},\boldsymbol{n}}, \boldsymbol{R}^{\boldsymbol{V},\boldsymbol{n}})}{\boldsymbol{\partial\varphi}, \boldsymbol{V}}^{-1} \cdot \begin{bmatrix} \mathbf{R}^{\boldsymbol{\varphi},\mathbf{n}} \\ \mathbf{R}^{\mathbf{V},\mathbf{n}} \end{bmatrix} \right)$$

   where the partial derivatives and the residual expressions are evaluated at $({}^{\boldsymbol{k}}\boldsymbol{\varphi}^{\boldsymbol{n+1}}, {}^{\mathbf{k}}\mathbf{V}^{\mathbf{n+1}}, {}^{\mathbf{k}}\mathbf{F}^{\mathbf{act,n+1k}}\mathbf{h}^{\mathbf{n+1}})$.

Thus, to iterate the Newton-Raphson's algorithm, we will have to compute the partial derivatives of the residual equations.

$$\frac{\boldsymbol{\partial}(\boldsymbol{R}^{\boldsymbol{\varphi},\boldsymbol{n}}, \boldsymbol{R}^{\boldsymbol{V},\boldsymbol{n}})}{\boldsymbol{\partial\varphi}, \boldsymbol{V}} = \begin{bmatrix} \boldsymbol{K}^{\boldsymbol{\varphi},\boldsymbol{\varphi}} & \boldsymbol{K}^{\boldsymbol{\varphi},\boldsymbol{V}} \\ \boldsymbol{K}^{\boldsymbol{V},\boldsymbol{\varphi}} & \boldsymbol{K}^{\boldsymbol{V},\boldsymbol{V}} \end{bmatrix}$$

Since we do not consider stretch activated channels and stretch-induced change in the propagation speed, R^V will never depend on $\boldsymbol{\varphi}$, so $\frac{\partial R^V}{\partial \boldsymbol{\varphi}} = \boldsymbol{K}^{\boldsymbol{V},\boldsymbol{\varphi}} = 0$. In the other cases,

$$\begin{aligned}
\boldsymbol{K}^{\boldsymbol{\varphi},\boldsymbol{\varphi}}{}_{I,J} &= \int_\Omega \nabla N_I \cdot \frac{\partial \mathbf{P}}{\partial \mathbf{F}} \nabla N_J d\Omega \\
\boldsymbol{K}^{\boldsymbol{\varphi},\boldsymbol{V}}{}_{I,L} &= \int_\Omega \nabla N_i \cdot \frac{\partial \mathbf{P}^{\mathbf{act}}}{\partial V} N_l \, d\Omega \\
\mathbf{K}^{\mathbf{V},\mathbf{V}}{}_{K,L} &= 1/\Delta t \int_\Omega N_k N_l \, d\Omega + \int_\Omega \nabla N_k \cdot (D \cdot \nabla N_l) \, d\Omega + \int_\Omega N_k \frac{\partial g_v}{\partial V} N_l d\Omega
\end{aligned}$$

3.2 Staggered resolution of the coupled problem

A more simplified, but faster alternative way of computing how the wave propagation affects into the contraction for a case that does not take into account the stretch activity channels and the stretch-induced change in the propagation speed, is a staggered resolution of the problem. In this case, we first solve the potential problem and then we apply the results to the mechanical one. The iterative structure of it at each time step is:

1. Given $(\boldsymbol{\varphi}^{\boldsymbol{n}}, \mathbf{V}^{\mathbf{n}}, \mathbf{F}^{\mathbf{act,n}}, \mathbf{h}^{\mathbf{n}})$ from the previous time step, we define $({}^{\mathbf{0}}\boldsymbol{\varphi}^{\boldsymbol{n+1}}, {}^{\mathbf{0}}\mathbf{V}^{\mathbf{n+1}}) = (\boldsymbol{\varphi}^{\boldsymbol{n}}, \mathbf{V}^{\mathbf{n}})$,
2. While $||\mathbf{R}^{\mathbf{V,n}}({}^{\mathbf{k}}\mathbf{V}^{\mathbf{n+1}}, {}^{\mathbf{k}}\mathbf{h}^{\mathbf{n+1}}))|| > tol^V$,
   (a) We compute ${}^{\mathbf{k+1}}\mathbf{h}^{\mathbf{n+1}}$ using Eq. 29,
   (b) We update the variables ${}^{\mathbf{k+1}}\mathbf{V}^{\mathbf{n+1}}$ applying the Newton-Raphson's method,

$$ {}^{\mathbf{k+1}}\mathbf{V}^{\mathbf{n+1}} = {}^{\mathbf{k}}\mathbf{V}^{\mathbf{n+1}} - \mathbf{K}^{\mathbf{VV}^{-1}}\mathbf{R}^{\mathbf{V,n}} $$

   where the partial derivative and the residual expression are evaluated at $({}^{\mathbf{k}}\mathbf{V}^{\mathbf{n+1}}, {}^{\mathbf{k}}\mathbf{h}^{\mathbf{n+1}})$.
3. While $||(\mathbf{R}^{\boldsymbol{\varphi},\mathbf{n}}({}^{\boldsymbol{k}}\boldsymbol{\varphi}^{\boldsymbol{n+1}}, \mathbf{V}^{\mathbf{n+1}}, {}^{\mathbf{k}}\mathbf{F}^{\mathbf{act,n+1}})|| > tol^{\varphi}$,
   (a) We compute $({}^{\mathbf{k+1}}\mathbf{F}^{\mathbf{act,n+1}}$ using Eq. 28 ,
   (b) We update the variables ${}^{\boldsymbol{k+1}}\boldsymbol{\varphi}^{\boldsymbol{n+1}}$ applying the Newton-Raphson's method,

$$ {}^{\boldsymbol{k+1}}\boldsymbol{\varphi}^{\boldsymbol{n+1}} = {}^{\mathbf{k}}\varphi^{\mathbf{n+1}} - \mathbf{K}^{\varphi\varphi^{-1}}\mathbf{R}^{\boldsymbol{\varphi},\mathbf{n}} $$

   where the partial derivative and the residual expression are evaluated at $({}^{\boldsymbol{k}}\boldsymbol{\varphi}^{\boldsymbol{n+1}}, \mathbf{V}^{\mathbf{n+1}}, {}^{\mathbf{k}}\mathbf{F}^{\mathbf{act,n+1}})$.

Note that in this case, we can also solve the electrophysiological problem for all the time steps, and then we can apply this data to solve the mechanical solution.

Another advantage is that, we can consider different time steps for the two resolutions ($\Delta t^V < \Delta t^{\varphi}$) if we do not want so much detail on the mechanical part. We can solve the electrical part, and after that solve the mechanical part actualizing the position every n iterations of the electrical solution, then $\Delta t^{\varphi} = n\Delta t^V$.

Parameter	V_C	ϵ	τ_0	τ_A	τ_-	τ_+
Value	0.1	0.005	150	6	60	12

Table 1: Used parameter for the electrophysiological model

Parameter	k_F	V_r	$\bar{V}$	ϵ_0	ϵ_∞	ξ	ν	E
Value	15	0	0.1	1	0.1	100	0.35	100

Table 2: Used parameter for the simulations of the coupled electromechanical model

4 Results

In this section we will present the resulting simulations of the electrical model, and of the coupled electromechanical model for a $3cm \times 3cm \times 0.5cm$ cardiac tissue. For the first model, we will consider 3 different meshes of cubic elements. For the second case, we will apply the staggered methodology that we explained in section 3.2 to the plane wave.

For the simulations we used the parameters that we can see in Tab. 1 and Tab. 2.

4.1 Electrophysiological model

In this case, we studied the convergence of the solution for electric model for an isotropic case considering 3 cubic meshes with different element sizes: $\Delta x = 0.5/2cm$ then $12 \times 12 \times 2 = 288$ elements, $\Delta x = 0.5/3cm$ then $18 \times 18 \times 3 = 972$ elements and $\Delta x = 0.5/4cm$ then $24 \times 24 \times 4 = 2304$ elements.

As initial conditions, we considered that $\Omega \cap \{x = 0\}$ was equal to $(V_0, h_0) = (0.2, 0.4)$ and $(V_0, h_0) = (0, 0)$ otherwise.

As result we had the expected results as we can see in Fig. 11 and Fig. 13. In the first one, the change of potential in the central node (located at $(1.5, 1.5, 0.25)$) as function of time is represented for the 3 different meshes. We can observe the convergence for the finest mesh to an smoother curve that behaves as Fig.9. In the second one, we represent the potential in the whole tissue in 4 different time instants using the finest mesh. We can see that the electrical wave propagates along the tissue in a sharped front, the highest potential covers all the tissue and then it returns to the resting state in a smoother way.

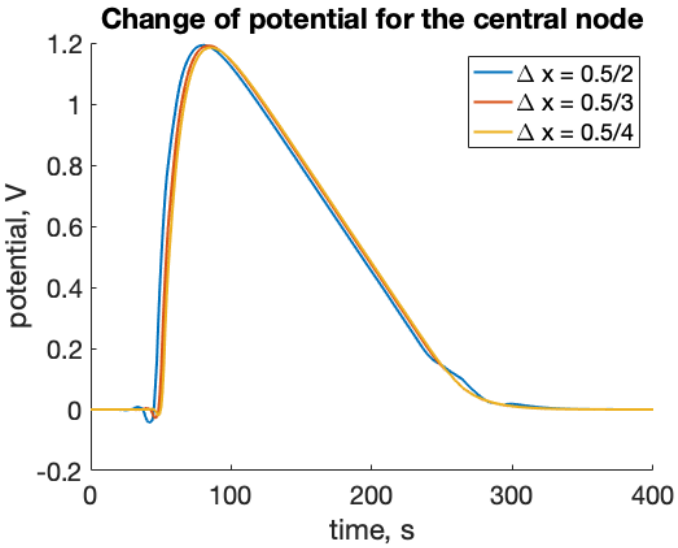

Figure 11: Potential as a function of time for the central node for 3 different meshes.

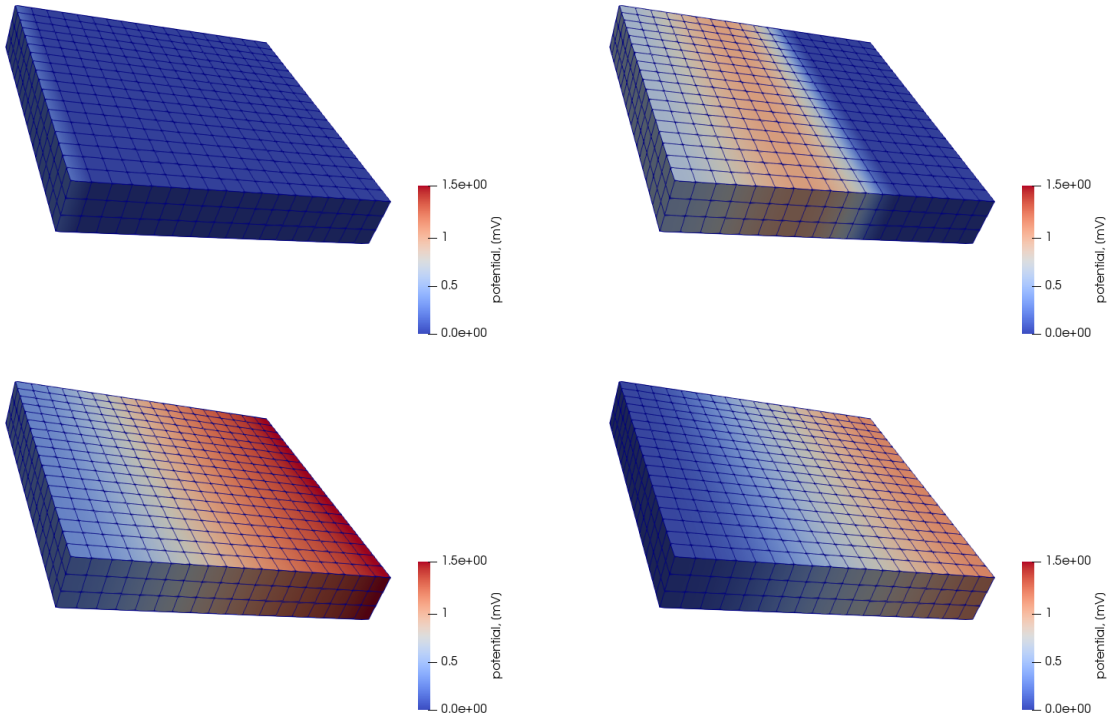

Figure 12: Simulation of the electrophysiological model at $t_0 = 0ms$, $t_{600} = 60ms$, $t_{1200} = 120ms$ and $t_{1800} = 180ms$.

4.2 Resolution of the coupled model

In this section we tried to develop a code that computed the resolution using the full implicit methodology, but at the end of the project, due to errors in the code, simulations did not converge to a solution. Instead of the full implicit resolution, we finally applied the staggered method that was explained in section 3.2.

In this case, we applied the same initial conditions for the electrical part, we fixed the node with initial coordinates $(L_x/2, L_y/2, 0)$, and we fixed the x and y movements for the nodes above, i.e. the ones with initial coordinates $(L_x/2, L_y/2, n/6)$ with $n = 1, 2, 3$.

The obtained results, that we can see in Fig. 13 and Fig. 14, show us how the change of potential affects on the contraction of muscle. We can observe that acts after the electrical wave front passes and turns back to the initial position when the potential returns to the resting state.

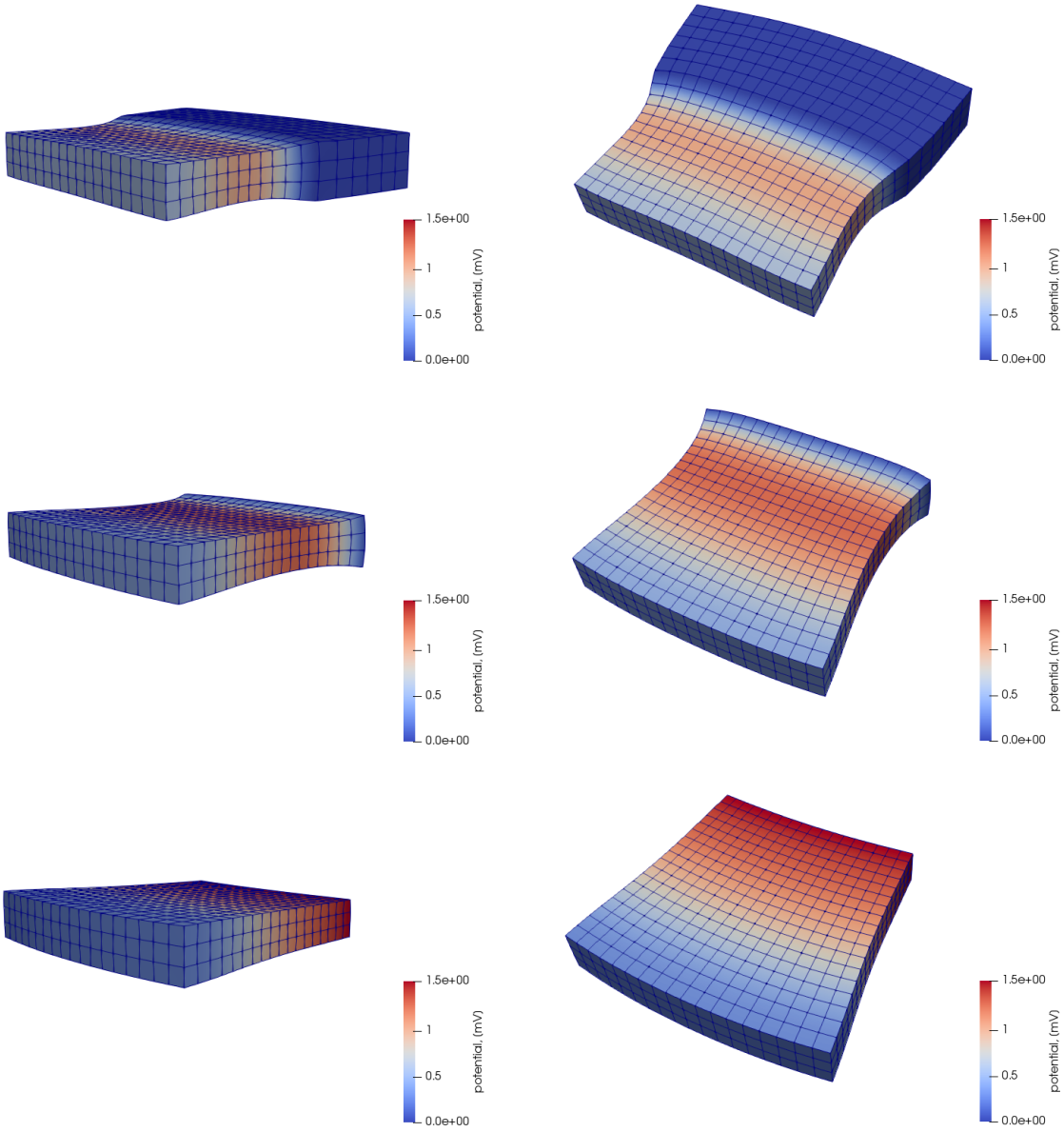

Figure 13: Simulation of the potential for the electromechanical model at $t_{60} = 60ms$ (first row), $t_{90} = 120ms$ (second row) and $t_{120} = 120ms$ (third row).

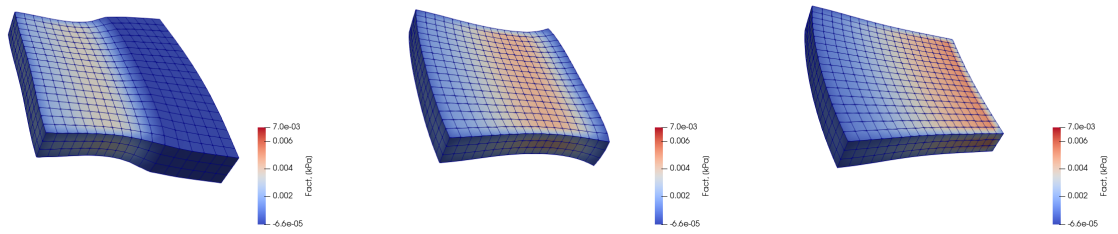

Figure 14: Simulation of the active tension for the electromechanical model at $t_{60} = 60ms$ (first picture), $t_{90} = 120ms$ (second picture) and $t_{120} = 120ms$ (third picture).

5 Conclusions and future work

In this project, we implemented a FEM code that solves the electrophysiological problem on a three dimensional piece of tissue. Even though it has some errors in the coding, we raised and develop a code that solves using a full implicit method the electromechanical model. We also present a faster, but less accurate alternative using a staggered methodology: first computing the potential and then using it to compute the variation of shape of the tissue due the active tension that is induced by this change.

As future work, we can state a lot of possibilities.

First of all, of course, solving the errors that has the full implicit algorithm and compare its results with the ones that the staggered algorithm offers, searching the accuracy limits of the last one.

We can also use more realistic electromechanical models that include the concentration of calcium as a variable, as we know that is what really causes the activation of the active tension, and/or that include how the contraction affects on the potential propagation, with stretch activity channels or the stretch-induced change in the propagation speed.

Another possible continuation of the project, could be to simulate more interesting situations as spiral waves, that are closely related to tachycardia and its transition to fibrillation.

Finally, we could also use this methodology to simulate the electromechanical wave propagation on a more realistic geometry as they did in [11] and in [12].

References

[1] Malmivuo, Plonsey, Jaakko Malmivuo, and Robert Plonsey. Bioelectromagnetism: principles and applications of bioelectric and biomagnetic fields. Oxford University Press, USA, 1995.

[2] Alonso, Sergio, Markus Bär, and Blas Echebarria. "Nonlinear physics of electrical wave propagation in the heart: a review." Reports on Progress in Physics 79.9 (2016): 096601.

[3] PJ Hunter, AD McCulloch, and HEDJ ter Keurs. "Modelling the mechanical properties of cardiac muscle." Progress in Biophysics and Molecular Biology, 69(2-3):289–331, 1998.

[4] Martyn P Nash and Alexander V Panlov. "Electromechanical model of excitable tissue to study reentrant cardiac arrhythmias." Progress in Biophysics and Molecular Biology, 85(2):501–522, 2004.

[5] Noble, Denis. "A modification of the Hodgkin—Huxley equations applicable to Purkinje fibre action and pacemaker potentials." The Journal of physiology 160.2 (1962): 317-352.

[6] Beeler, G. W., and H. Reuter. "Membrane calcium current in ventricular myocardial fibres." The Journal of physiology 207.1 (1970): 191-209.

[7] Flavio H. Fenton and Elizabeth M. Cherry (2008) Models of cardiac cell. Scholarpedia, 3(8):1868.

[8] Echebarria, Blas, and Alain Karma. "Spatiotemporal control of cardiac alternans." Chaos: An Interdisciplinary Journal of Nonlinear Science 12.3 (2002): 923-930.

[9] Pandit, Sandeep V., et al. "A mathematical model of action potential heterogeneity in adult rat left ventricular myocytes." Biophysical journal 81.6 (2001): 3029-3051.

[10] Vladimir S. Zykov (2008) Excitable media. Scholarpedia, 3(5):1834.

[11] Wong, Jonathan, Serdar Göktepe and Ellen Kuhl. "Computational modeling of electrochemical coupling: A novel finite element approach towards ionic models for cardiac electrophysiology." (2011).

[12] Dal, Hüsnü, Göktepe, Serdar , Kaliske, Michael and Kuhl, Ellen. (2013). A fully implicit finite element method for bidomain models of cardiac electromechanics. Computer Methods in Applied Mechanics and Engineering. 253. 323-336. 10.1016/j.cma.2012.07.004.

[13] Holzapfel, G.A. Meccanica (2002) 37: 489. https://doi.org/10.1023/A:1020843529530

[14] Bers, Donald. (2002). Bers, DM. Cardiac excitation-contraction coupling. Nature 415: 198-205. Nature. 415. 198-205. 10.1038/415198a.